PHYSICAL REVIEW FLUIDS 2, 081301(R) (2017)

Analog of discontinuous shear thickening flows under confining pressure

Junhao Dong and Martin Trulsson
Theoretical Chemistry, Department of Chemistry, Lund University, Lund, Sweden
(Received 25 January 2017; published 30 August 2017)

We use two-dimensional numerical simulations to study dense suspensions of non-Brownian hard particles using the Critical Load Model (CLM) under constant confining pressures. At constant packing fraction this simple model shows shear thickening as the tangential forces get activated upon increased shear stresses. By parameterizing a simple binary system of frictional and nonfrictional particles of different proportions we show that the jamming packing fraction, at which the viscosity diverges, is controlled by the fraction of frictional contacts. The viscosity of dense suspensions can thereby be expressed as a function of the fraction of frictional contacts as well as the packing fraction of solid particles. In addition, we show that there exists a simple relationship between the fraction of frictional contacts and the two control parameters (under confining pressure): the viscous number J and the ratio between the repulsive barrier force and confining pressure. Under confining pressures the viscosity curves are found to depend on the shear protocol, with the possibility of yielding negative *dynamic* compressibility, an analog to the discontinous shear thickening found at high but constant packing fractions for the same system.

DOI: 10.1103/PhysRevFluids.2.081301

Dense suspensions of rigid particles are of great importance from both a geological and an industrial point of view, including materials such as mud, quicksand, slurry, tooth-paste, paint, etc. Such suspensions show a variety of rheological behaviors, and a substantial amount of research has been done trying to facilitate our understanding of these behaviors [1–7].

In the simplest model describing non-Brownian suspensions, where particles are assumed to have no inertia or Brownian motion and being immersed in a highly viscous fluid, the suspension's viscosity will be a sole function of packing fraction ϕ and the fluid viscosity [4]. While the viscosity of dilute suspensions is given by the hydrodynamic stresses on single particles in a shear flow and distant hydrodynamic interactions between pairs [1] the viscosity in dense suspensions is governed by viscous dissipation due to particle departures from the affine flow due to geometrical constraints [8–10]. The path of departures will increase as the packing fraction increases and finally diverge at the jamming transition. While this is a good model for most of suspensions, it does not include the possibility of shear thinning or shear thickening. The latter phenomenon has lately attracted an increasing interest in basic research. In these suspensions the viscosity increases as a function of shear rate [11]. This increase is labeled as continuous or discontinuous depending on how significant and how sharp the increase is. Transition with significant and sharp viscosity increase is defined as discontinuous shear thickening (DST). DST is usually observed when packing fraction of the suspension exceeds a certain threshold while a lower packing fraction gives a more continuous shear thickening [12]. Several scenarios have been proposed to explain shear thickening behavior. It is known that the inertia of the particles [13] and/or fluid [14] gives a continuous shear thickening (CST) above a certain shear rate, usually described by the Stokes and/or Reynolds number(s). However, other scenarios are also proposed to explain shear thickening with inertia being subdominant.

Hydroclustering has been a dominating explanation for a couple of decades, where shear thickening is driven by clustering of particles upon increasing shear rate leading to effectively larger quasiparticles. These transient hydroclusters have little internal rearrangement but a large collective rotational and translational movement which leads to a high dissipation, hence increased viscosity [2,15]. Although hydroclustering works well in describing weak shear thickening, simulations based on this phenomenon have not been able to produce the dramatic viscosity increase observed in discontinuous shear thickening [5].

Another alternative explanation consider friction contact as driven force of shear thickening. Several recent papers justify the contributions of friction contact to shear thickening both experimentally [16,17] and computationally [18–20]. Shear thickening is due to the onset of tangential force with increasing shear rate or, equivalently increasing stresses [12,21]. It is now well studied that the rheology of frictional and nonfrictional dense suspension differ in the jamming packing fraction and the viscosity at the same shear rate, where frictional suspensions diverge at lower packing fractions and have higher viscosities at the same packing fraction compared to nonfrictional suspensions [22]. The former results from a counting argument where extra frictional forces can mechanically stabilize the packings with fewer contacts per particle, hence lower packing fractions. These extra tangential forces also increase the dissipation and hence the viscosity. In this explanation, particles are initially stabilized by repulsive or lubricative forces, e.g., electrostatic force and/or steric force, thus being regarded as nonfrictional dense suspension. As shear rate increases, particles obtain enough energy to overcome the barrier and frictional contacts are therefore "activated." Shear thickening behavior is explained as transitions from nonfrictional suspension to frictional suspension.

Although there has been a lot of attention following this explanation or model, most works have been done under constant packing fraction [12,22–24], and very little is known about how these suspensions behave under constant confining pressure where packing fractions are allowed to adapt freely, which might be a more relevant boundary condition for geological processes or nonplanar shear cells [25]. Such confining pressure conditions have previously been successfully used to investigate the physics of dense suspension close to jamming. It was first pioneered by Boyer *et al.* [4] allowing them to unify the rheology of granular material and dense suspensions. Using the same concept, Trulsson *et al.* [10] explored the crossover between Newtonian and Bagnoldian flows for non-Brownian suspensions. Recently, Wang and Brady [26] studied the flow-arrested transition for Brownian suspensions with the same concept.

In our work, we explore behavior of dense suspensions under confining pressure based on the scenario of "activation" of frictional contacts. We focus on non-Brownian suspensions in highly viscous fluids. Besides of finding relations between viscosity, packing fraction and fraction of frictional contact, we also explore different shear protocols yielding different viscosity versus packing fraction curves.

Simulations are run in two dimensions with a constant number of disks, $N_{\rm p} = 948$, with average diameter d and polydispersity $\pm 50\%$ to avoid crystallization. Periodic boundary condition is applied along the x direction. The cell size is approximately $47d$ in the x direction (along the shear) but is allowed to vary in the other direction (typically $\sim 20d$). The disks are confined between two rough walls and immersed in a highly viscous fluid with viscosity η_0. The disk dynamics is hence strictly overdamped without Brownian noise, which gives us a set of equations of force and torque balance for each disk i. The force balance is given as $\vec{F}_i^{\rm ext} + \vec{F}_i^{\rm v} - \sum_j \vec{f}_{ij} = 0$, where $\vec{F}^{\rm ext}$ is the external force from walls, $\vec{F}^{\rm v}$ is the viscous drag force, and $\vec{f}_{ij}$ is the contact force exerted on disk j by disk i. The drag force is given by the sum of Stokes drag and Archimedes force; $\vec{F}_i^{\rm v} = -\frac{3\pi\eta_0}{1-\phi_0}(\vec{V}_i - \vec{V}_i^{\rm a})$, where $\vec{V}_i^{\rm a} = \dot{\gamma} y \hat{x}$ is the affine fluid velocity at a shear rate $\dot{\gamma}$ and $\phi_0 = 0.76$ a constant used to scale the drag contributions according to experiments. Similarly, the torque balance is $\tau_i^{\rm ext} + \tau_i^{\rm v} - \sum_j \tau_{ij} = 0$. The force between two disks consists of two components: normal force $\vec{f}_{\rm n}$ and tangential force $\vec{f}_{\rm t}$. Here we assume elastic stiff disks in our simulation so the normal force is given by a linear force, $f_{\rm n}^{ij} = k_{\rm n}\delta_{\rm n}^{ij}$, where $\delta_{\rm n}^{ij}$ is the overlap between two disks and $k_{\rm n}$ is the normal spring constant. The tangential force is obtained in a similar way but using tangential spring and a tangential spring constant $k_{\rm t} = 0.5k_{\rm n}$. The relation between normal component and tangential component is constrained by Coulomb friction, $|f_{\rm t}| \leqslant \mu_{\rm p}|f_{\rm n}|$, where $\mu_{\rm p}$ is the friction coefficient (for more information see, e.g., Ref. [27]). In all of our simulations we put $\mu_{\rm p} = 1$. The lubrication force is not considered here since it will cause only a minor difference in the final results (see Sec. B of the Supplemental Material [28] for more details), such an observation is consistent with recent experiments [16] and simulations [19], where contact forces are found to be the dominant forces in a steady state.

We use two different models, the Critical Load Model and a binary model. The Critical Load Model (CLM) has been successful in generating both CST and DST behaviors [6,12,24] by allowing contacts to switch between lubricative (nonfrictional) and frictional states. The model constitutes of a critical normal force $f_{\mathrm{n}}^{\mathrm{cl}}$ which represents the magnitude of the repulsive force between two disks at which frictional contacts set in. The friction coefficient between disk i and j is then determined by comparing the normal force between two disks with $f_{\mathrm{n}}^{\mathrm{cl}}$:

$$\mu_{\mathrm{p}}^{ij} = \begin{cases} \mu_{\mathrm{p}}, & f_{\mathrm{n}}^{ij} > f_{\mathrm{n}}^{\mathrm{cl}} \\ 0, & f_{\mathrm{n}}^{ij} < f_{\mathrm{n}}^{\mathrm{cl}}. \end{cases} \tag{1}$$

Accordingly, a contact is defined as frictional when $\mu_{\mathrm{p}}^{ij} = \mu_{\mathrm{p}}$; otherwise, it is frictionless. In this way, the frictional contacts are able to be "activated" or "deactivated" during simulation. We define the fraction of frictional contact χ_{f} as the ratio between the number of contacts being frictional and the total number of contacts. In order to better understand the influence of χ_{f} on jamming packing fractions and flow curves, we also run a conceptual system where χ_{f} are restricted. The system is a binary mixture of ideally smooth disks (i.e., $\mu_{\mathrm{p}}^{i} = 0$) and rough disks (i.e., $\mu_{\mathrm{p}}^{i} = \mu_{\mathrm{p}}$).

The friction coefficient between disk i and j is defined as $\mu_{\mathrm{p}}^{ij} = \sqrt{\mu_{\mathrm{p}}^{i}\mu_{\mathrm{p}}^{j}}$ (i.e., only between two rough disks can one have frictional contacts). In this way, it is easy to control the fraction of frictional contacts by controlling the fraction of rough disks as $\chi_{\mathrm{f}} \simeq (\frac{N_{\mathrm{f}}}{N_p})^2$ where N_f is the number of rough disks (validated in Sec. A of the Supplemental Material [28]).

The simulations are shear rate-controlled, by imposing constant velocities of the walls, either at constant packing fraction or constant pressure. The latter is fulfilled by imposing a constant pressure P to both walls, allowing the shear cell to dilate or compress during the shearing. The velocities of fluid and disks follow the linear profile, with slope $\dot{\gamma}$, set by the viscous fluid. All the measurements are done considering only the central part of the shear cell, excluding five layers of disks close to each wall, over a total strain $\gamma = \dot{\gamma}t$ of 3 to 10 d. In our simulation, we vary the viscous number $J \equiv \eta_0\dot{\gamma}/P$ by changing either the confining pressure P or the shear rate $\dot{\gamma}$ and measure how the viscosity $\eta = \sigma/\dot{\gamma}$, where σ is shear stress, and χ_{f} changes with J. The stiffness of disks is maintained by keeping $k_{\mathrm{n}}/P \approx 2 \times 10^3$ (giving in principle a hard disk behavior). To get more systematic understanding, we run simulations with either $f_{\mathrm{n}}^{\mathrm{cl}}/(Pd)$ or $f_{\mathrm{n}}^{\mathrm{cl}}/(\eta_0\dot{\gamma}d)$ constant corresponding to two different shear protocols: keeping either P constant and varying $\dot{\gamma}$ or keeping $\dot{\gamma}$ constant and varying P. We also run two reference simulations; in one case, all contacts are frictional (i.e., $f_{\mathrm{n}}^{\mathrm{cl}} = 0$), while in the other case, all contacts are frictionless (i.e., $f_{\mathrm{n}}^{\mathrm{cl}} = \infty$).

To validate that the model used is able to reproduce shear thickening behavior (by "activation" of frictional contact), we first run the simulation with five constant packing fractions $\phi = 0.43, 0.54, 0.63, 0.76, 0.79$. We plot reduced viscosity η/η_0 as a function of dimensionless shear rate $\dot{\gamma}\eta_0/(f_{\mathrm{n}}^{\mathrm{cl}}d)$ (see Sec. A of the Supplemental Material [28]). All the curves clearly show shear-thickening behavior when the shear rate reaches a critical value $\dot{\gamma}_0$. At $\phi = 0.43$, the continuous increase is quite small. As ϕ increases, the shear thickening becomes more pronounced both in magnitude and in sharpness and eventually becomes discontinuous. This result is consistent with previous reported works [12,22].

We then run simulations with a constant confining pressure P and study how the reduced viscosity η/η_0 changes with packing fraction ϕ. Divergence of dense suspension close to jamming can be estimated as

$$\eta/\eta_0 \simeq k(\phi_{\mathrm{c}} - \phi)^{-m}, \tag{2}$$

where ϕ_{c} is critical packing fraction where jamming transition happens. For a constant χ_{f}, ϕ is a function of J [4]; $\phi \to \phi_{\mathrm{c}}$ when $J \to 0$. Since frictional contact will influence packing of disks, it is reasonable to think that $\phi_{\mathrm{c}} = \phi_{\mathrm{c}}(\chi_{\mathrm{f}})$ and bound by the two limits $\phi_{\mathrm{c}}(0) = \phi_{\mathrm{c}}^{\mathrm{nf}}$ and $\phi_{\mathrm{c}}(1) = \phi_{\mathrm{c}}^{\mathrm{f}}$, where the subscripts denote either the fully frictional or nonfrictional references. All intermediate

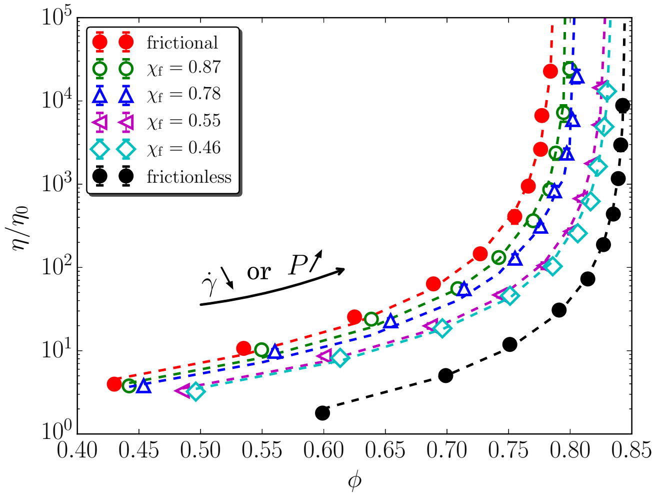

FIG. 1. Reduced viscosity η/η_0 as a function of packing fraction ϕ for various χ_f. Symbols are simulation results and dashed lines are plots of Eq. (4) with corresponding χ_f.

χ_f cases can then be expressed as

$$\phi_c(\chi_f) = \phi_c^f g(\chi_f) + \phi_c^{nf}[1 - g(\chi_f)], \tag{3}$$

where $g(\chi_f) \in [0,1]$ is a combination function conjectured by Wyart and Cates [22]. Furthermore, we assume that $k = k(\chi_f)$ and $m = m(\chi_f)$ can be expressed in a corresponding way as for $\phi_c(\chi_f)$ so that

$$\eta/\eta_0 = \eta(\phi,\chi_f) = k(\chi_f)[\phi_c(\chi_f) - \phi]^{-m(\chi_f)}. \tag{4}$$

To test our assumption, we first run simulations with constant χ_f (binary system). The results are plotted in Fig. 1. We fit the data using Eq. (2) and get a set of ϕ_c corresponding to different χ_f. We now fit these data to Eq. (3) with $g(\chi_f) = \chi_f^{b_{\phi_c}}$ and $b_{\phi_c} \simeq 2$. We apply the same strategy to k and m and get $b_k \simeq 0.4$ and $b_m \simeq 2.2$, respectively (fits are presented in Sec. A of the Supplemental Material [28]). Since we have expressions for $k(\chi_f)$, $\phi_c(\chi_f)$, and $m(\chi_f)$, we now plot Eq. (4) with corresponding χ_f. The plots are presented in Fig. 1 as dashed lines, which shows that Eq. (4) fit well with simulation data. This indicates that our assumption works well to predict viscosity for given ϕ and χ_f [29].

Now we apply the same assumptions to the CLM model. Figure 2 shows both simulation results and plots using Eq. (4) with parameters from the binary system with ϕ and χ_f measured from simulations with astonishing agreement and shows a robustness of these reduced parameters (i.e., data from CLM model can be mapped to binary system with the same viscous number J and fraction of frictional contact χ_f) irrespectively of the detailed microscopic structure (results of two specific cases are shown in Table I; for corresponding snapshots, see Sec. A of the Supplemental Material [28]).

For both shear protocols (keeping constant either $f_n^{cl}/(Pd)$ or $f_n^{cl}/[\dot{\gamma}\eta_0 d)]$, curves show a tendency of crossing between the frictional and frictionless branches. Notice that the two shear protocols generate different types of transition: keeping $f_n^{cl}/(Pd)$ constant yields curves with transition from the frictional to the frictionless branch, while the opposite trend is observed for the other shear protocol. For constant $f_n^{cl}/(Pd)$, both η/η_0 and ϕ increase as shear rate $\dot{\gamma}$, and hence J, decreases. Similar results are found controlling $f_n^{cl}/(\dot{\gamma}\eta_0 d)$ if the parameter is low enough (typically $\lesssim 300$). On the other hand, for high and constant $f_n^{cl}/(\dot{\gamma}\eta_0 d)$, one finds cusp-shaped behaviors with an increasing cusp as $f_n^{cl}/(\dot{\gamma}\eta_0 d)$ increases. For these cups one finds two (or more) viscosities for each packing fraction (except possibly at the maximum ϕ). These two states do,

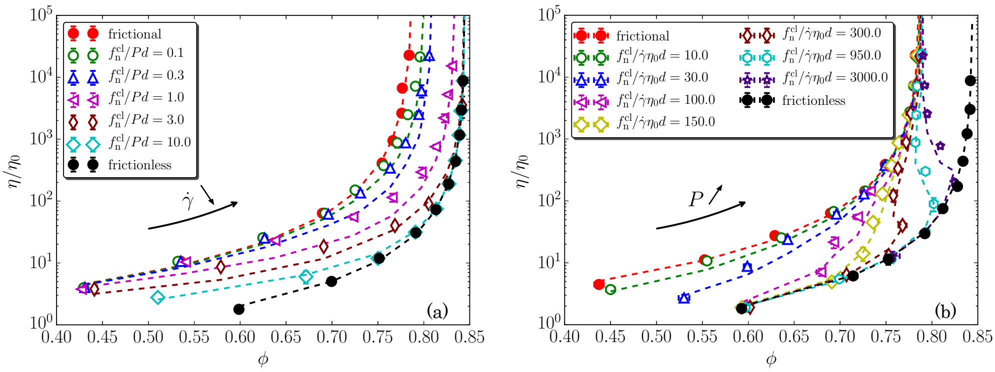

FIG. 2. Reduced viscosity η/η_0 as a function of packing fraction ϕ with two different shear protocols, (a) keeping $f_n^{cl}/(Pd)$ constant (i.e., varying $\dot{\gamma}$), (b) keeping $f_n^{cl}/(\dot{\gamma}\eta_0 d)$ constant (i.e., varying P). Symbols are simulation results, and dashed lines are plots of Eq. (4).

however, have different pressures (assuming fixed f_n^{cl}), with a higher pressure for the high-viscosity case. For example, at $f_n^{cl}/(\dot{\gamma}\eta_0 d) = 3000$ and $\phi \simeq 0.81$ we find that the high-viscosity state has a pressure 10 times larger than the low-viscosity state. These dual states can also be observed when plotting ϕ versus J; see Fig. 3(b). This indicates a range of pressures where one has a negative *dynamic* compressibility, i.e., ϕ decreases with increasing P. The negative *dynamic* compressibility is more obviously illustrated in Fig. 3(b) where one observes nonmonotonic behaviors in ϕ as a function of P (i.e., having both positive and negative compressibilities). This appears when ϕ is above ϕ_c^f since then $\phi_c^f < \phi < \phi_c \leqslant \phi_c^{nf}$; as χ_f increases with P (for more discussion about Fig 3, see Sec. A of the Supplemental Material [28]) so must ϕ_c decrease to reach ϕ_c^f, yielding a negative *dynamic* compressibility.

Unlike in our reference binary system, χ_f is not controlled in the CLM model. Instead it is allowed to varied with J, and the control parameter as determined by the shear protocol (as seen in Sec. A of the Supplemental Material [28]). It is, however, reasonable to presume that χ_f is related to $f_n^{cl}/\langle f_n \rangle$ according to the presumption of the CLM model, where $\langle f_n \rangle$ is the average of normal force between two disks. Given that $P \sim \langle f_n \rangle$, we assume $\chi_f = \chi_f[f_n^{cl}/(Pd), J]$. As $\lim_{J\to 0} \phi = \phi_c$ and given that $\phi_c = \phi_c(\chi_f)$, we can assume $\phi = \phi[f_n^{cl}/(Pd), J]$. These assumptions are tested, and we obtain expressions for χ_f and ϕ by fitting corresponding simulation data (see Sec. A of the Supplemental Material). Now we can rewrite Eq. (4) as

$$\eta = \eta\big(f_n^{cl}/Pd, J\big). \tag{5}$$

Remembering that $J \equiv \dot{\gamma}\eta_0/P$, one can reexpress both previous control parameters in terms of J and $f_n^{cl}/(Pd)$: $f_n^{cl}/(Pd) = [f_n^{cl}/(Pd)]J^0$ and $f_n^{cl}/(\dot{\gamma}\eta_0 d) = [f_n^{cl}/(Pd)]J^{-1}$. This shows the generality of Eq. (5). Following the above reasoning we actually find a whole family of shear protocols that can be encoded in the new parameter

$$D \equiv \frac{f_n^{cl}}{Pd}\left(\frac{J}{J_0}\right)^{\alpha}, \tag{6}$$

TABLE I. Simulation results of two specific simulations with the same J and χ_f.

	Viscous number J	Packing fraction ϕ	Fraction of frictional contact χ_f	Relative viscosity η/η_0
Binary	$(1.20 \pm 0.20) \times 10^{-5}$	0.843 ± 0.001	0.119 ± 0.004	9500 ± 1800
CLM	$(1.30 \pm 0.16) \times 10^{-5}$	0.841 ± 0.001	0.124 ± 0.006	9200 ± 1200

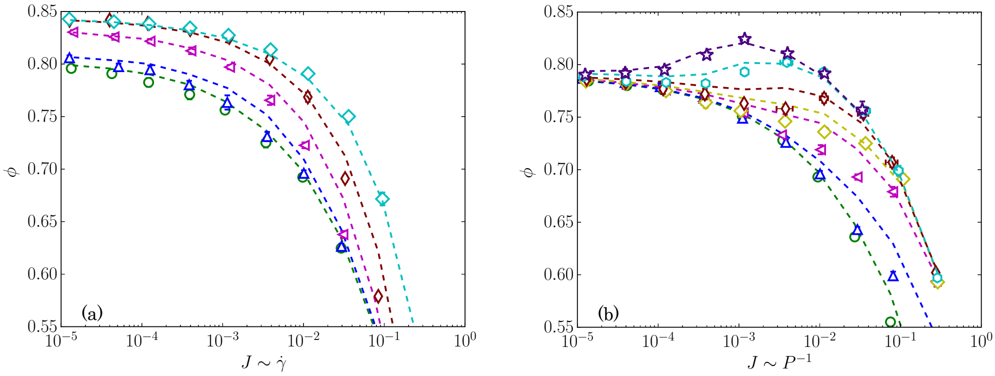

FIG. 3. Packing fraction ϕ as a function of viscous number J for various f_n^{cl}/Pd or $f_n^{cl}/\dot{\gamma}\eta_0 d$ with (a) varying $\dot{\gamma}$, (b) varying P; colors and styles of symbols are consistent with Fig. 2.

where J_0 is a reference point. With a given α, we can obtain a relation between J and P which can then be put into Eq. (5). Different α can be divided into three parts around the two previous reference points -1 and 0, which correspond to varying $\dot{\gamma}$ or varying P. The other α indicate that both $\dot{\gamma}$ and P are varied simultaneously. From Eq. (6) we see that pressure should be varied as $P \sim \dot{\gamma}^{\alpha/(1+\alpha)}$, and noticing that $J \sim \dot{\gamma}/P$ we can obtain $J \sim \dot{\gamma}^{1/(1+\alpha)}$. To observe divergence in viscosity (i.e., $J \to 0$ and consequently, $\phi \to \phi_c$), there are three possibilities to realize this. In the first case, both $\dot{\gamma}$ and P increase with P increasing more rapidly, which corresponds to $\alpha < -1$. In the second case, $\dot{\gamma}$ decreases while P increases, which corresponds to $-1 < \alpha < 0$. In the third cases, both $\dot{\gamma}$ and P decreases with P decreasing faster, which corresponds to $\alpha > 0$. These combinations of $\dot{\gamma}$ and P can be easily mapped to different shear protocols in experiments. Figure 4 illustrates plots of Eq. (5) with $J_0 = 0.001$ and $D = 1$ for various α. Frictional and frictionless curves are also produced by setting $D = 0$ and ∞, respectively. The choice of J_0 and D is by no means a unique choice but rather creates a common point in the $(\eta/\eta_0, \phi)$-space, or an equivalent the $(f_n^{cl}/(Pd), J)$-space, for

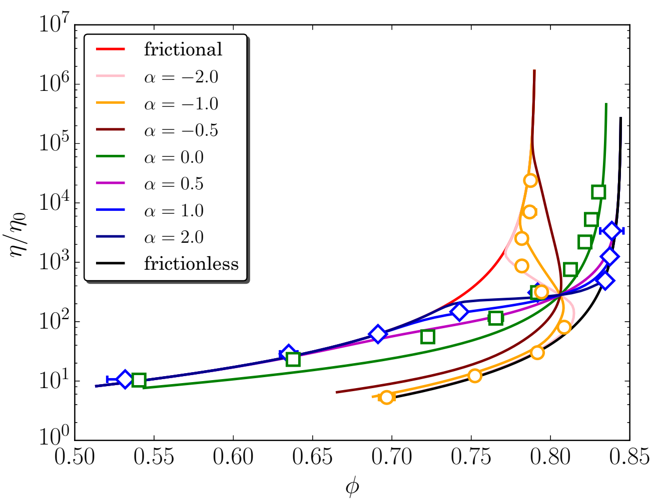

FIG. 4. Reduced viscosity η/η_0 as a function of packing fraction ϕ calculated from Eq. (5) for various α with $J_0 = 0.001$, $D = 1$; frictional and frictionless curves are produced by setting $D = 0$ and ∞. Symbols are simulation results for $\alpha = -1$ (circles), 0 (squares), and 1 (diamonds).

all different shear protocols and hence an intersection point. Simulation results corresponding to $\alpha = -1, 0$ and 1 are also shown in Fig. 4, which all show good agreements with the predictions from Eq. (5). Simulation results corresponding to $\alpha = 1$ with different D and J_0 can be found in Sec. A of the Supplemental Material [28]. Nonmonotonic curves are seen for both positive and negative α, where cusped curves become more significant with larger $|\alpha|$.

In this work, we simulate shear thickening of dense suspensions under confining pressure. By plotting $\eta(\phi)$ and fitting the data to the empirical equation $\eta/\eta_0 = \eta(\phi, \chi_f)$, we illustrate that both χ_f and ϕ determine the viscosity. In particular, the jamming point ϕ_c is determined by χ_f and hence the divergence of viscosity. We find different transition paths between the fully frictional and frictionless curves depending on the shear protocol. Negative *dynamic* compressibility is observed when varying P at $\phi > \phi_c^f$, resulting from a decreasing ϕ_c due to increasing χ_f. We further find that both χ_f and ϕ are functions of $f_n^{cl}/(Pd)$, which indicates that a relation between repulsive forces and confining pressure is a key factor of shear thickening behavior and could be used in continuum modeling. We also introduce a new dimensionless constant $D \equiv \frac{f_n^{cl}}{Pd}(\frac{J}{J_0})^\alpha$. Encoded in α is a whole set of different shear protocols, each generating its own flow curve. This observation could be tested and verified using current experiment protocols for shear-thickening suspensions [4]. So far we have assumed the particles being quasihard disks. Accounting also for elasto-hydrodynamics [30] would most likely generate even more complex flow behaviors as one now could have competing shear-thickening and shear-thinning behaviors. We aim to pursuit such studies in the future.

M.T. acknowledges financial support by the Swedish Research Council (621-2014-4387) and the Crafoord Foundation (20160568). The simulations were performed on resources provided by the Swedish National Infrastructure for Computing (SNIC) at the center for scientific and technical computing at Lund University (LUNARC). J.D. acknowledges Jasenko Gavran for initial help and instruction running the binary systems.

[1] G. K. Batchelor and J. T. Green, The determination of the bulk stress in a suspension of spherical particles to order c^2, J. Fluid Mech. **56**, 401 (1972).

[2] J. F. Brady and G. Bossis, Stokesian dynamics, Annu. Rev. Fluid Mech. **20**, 111 (1988).

[3] N. Wagner and J. F. Brady, Shear thickening in colloidal dispersions, Phys. Today **62**, 27 (2009).

[4] F. Boyer, É. Guazzelli, and O. Pouliquen, Unifying Suspension and Granular Rheology, Phys. Rev. Lett. **107**, 188301 (2011).

[5] E. Brown and H. M. Jaeger, Shear thickening in concentrated suspensions: Phenomenology, mechanisms, and relations to jamming, Rev. Prog. Phys. **77**, 046602 (2014).

[6] R. Mari, R. Seto, J. F. Morris, and M. M. Denn, Shear thickening, frictionless and frictional rheologies in non-Brownian suspensions, J. Rheol. **58**, 1693 (2014).

[7] C. D. Cwalina and N. J. Wagner, Material properties of the shear-thickened state in concentrated near hard-sphere colloidal dispersions, J. Rheol. **58**, 949 (2014).

[8] B. Andreotti, J.-L. Barrat, and C. Heussinger, Shear Flows of Non-Brownian Suspensions Close to Jamming, Phys. Rev. Lett. **109**, 105901 (2012).

[9] E. Lerner, G. Düring, and M. Wyart, Shear flows of non-Brownian suspensions close to jamming, Proc. Natl. Acad. Sci. USA **109**, 4798 (2012).

[10] M. Trulsson, B. Andreotti, and P. Claudin, Transition from the Viscous to Inertial Regime in Dense Suspensions, Phys. Rev. Lett. **109**, 118305 (2012).

[11] H. A. Barnes, Shear-thickening ("dilatancy") in suspensions of nonaggregating solid particles dispersed in Newtonian liquids, J. Rheol. **33**, 329 (1989).

[12] R. Seto, R. Mari, J. F. Morris, and M. M. Denn, Discontinuous Shear Thickening of Frictional Hard-Sphere Suspensions, Phys. Rev. Lett. **111**, 218301 (2013).

[13] R. A. Bagnold, Experiment on a gravity-free dispersion of large solid spheres in a newtonian fluid under shear, Prog. R. Soc. A **225**, 49 (1954).
[14] F. Picano, W.-P. Breugem, D. Mitra, and L. Brandt, Shear Thickening in Non-Brownian Suspensions: An Excluded Volume Effect, Phys. Rev. Lett. **111**, 098302 (2013).
[15] R. S. Farr, J. R. Melrose, and R. C. Ball, Kinetic theory of jamming in hard-sphere startup flows, Phys. Rev. E **55**, 7203 (1997).
[16] N. Y. C. Lin, B. M. Guy, C. Ness, M. Hermes, J. Sun, W. C. K. Poon, and I. Cohen, Hydrodynamic and Contact Contributions of Continuous Shear Thickening in Colloidal Suspensions, Phys. Rev. Lett. **115**, 228304 (2015).
[17] B. M. Guy, M. Hermes, and W. C. K. Poon, Towards a Unified Description of the Rheology of Hard-Particle Suspensions, Phys. Rev. Lett. **116**, 059901(E) (2016).
[18] C. Heussinger, Shear thickening in granular suspensions: Interparticle friction and dynamically correlated correlated cluster, Phys. Rev. E **88**, 050201 (2013).
[19] F. Peters, G. Ghigliotti, S. Gallier, F. Blanc, E. Lemaire, and L. Lobry, Rheology of non-Brownian suspensions of rough frictional particles under shear reversal: A numerical study, J. Rheol. **60**, 715 (2016).
[20] S. Gallier, F. Peters, E. Lemaire, and L. Lobry, Rheology of sheared suspension of rough frictional particles, J. Fluid Mech. **757**, 514 (2014).
[21] N. Fernandez, R. Mani, D. Rinaldi, D. Kadau, M. Mosquet, H. Lombois-Burger, J. Cayer-Barrioz, H. J. Herrmann, N. D. Spencer, and L. Isa, Microscopic Mechanism for Shear Thickening of Non-Brownian Suspensions, Phys. Rev. Lett. **111**, 108301 (2013).
[22] M. Wyart and M. E. Cates, Discontinuous Shear Thickening Without Inertia in Dense Non-Brownian Suspensions, Phys. Rev. Lett. **112**, 098302 (2014).
[23] R. Mari, R. Seto, J. F. Morris, and M. M. Denn, Nonmonotonic flow curves of shear thickening suspensions, Phys. Rev. E **91**, 052302 (2015).
[24] C. Ness and J. Sun, Shear thickening regimes of dense non-Brownian suspensions, Soft Matter **12**, 914 (2012).
[25] A. Fall, F. Bertrand, D. Hautemayou, C. Meziére, P. Moucheront, A. Lemaître, and G. Ovarlez, Macroscopic Discontinuous Shear Thickening Versus Local Shear Jamming in Cornstarch, Phys. Rev. Lett. **114**, 098301 (2015).
[26] M. Wang and J. F. Brady, Constant Stress and Pressure Rheology of Colloidal Suspensions, Phys. Rev. Lett. **115**, 158301 (2015).
[27] M. Trulsson, E. DeGiuli, and M. Wyart, Effect of friction on dense suspension flows of hard particles, Phys. Rev. E **95**, 012605 (2017).
[28] See Supplemental Material at http://link.aps.org/supplemental/10.1103/PhysRevFluids.2.081301 for snapshots, details about the fits, additional flow curves and simulation results considering lubrication force.
[29] Note that ϕ is not a control parameter in our pressure controlled systems but rather an observable (like η/η_0) and obtained by varying J and/or $f_{\mathrm{n}}^{\mathrm{cl}}/Pd$.
[30] S. Jamali, A. Boromand, N. Wagner, and J. Maia, Microstructure and rheology of soft to rigid shear-thickening colloidal suspensions, J. Rheol. **59**, 1377 (2015).